Atmos. Meas. Tech. Discuss., 5, 8653–8699, 2012
www.atmos-meas-tech-discuss.net/5/8653/2012/
doi:10.5194/amtd-5-8653-2012

Atmospheric Measurement Techniques Discussions

Ground-based remote sensing of thin clouds in the Arctic

T. J. Garrett[1] **and C. Zhao**[2]

[1]Department of Atmospheric Sciences, University of Utah, Salt Lake City, Utah, USA
[2]Lawrence Livermore National Laboratories, Livermore, California, USA

Received: 5 November 2012 – Accepted: 20 November 2012 – Published: 30 November 2012

Correspondence to: T. J. Garrett (tim.garrett@utah.edu)

Published by Copernicus Publications on behalf of the European Geosciences Union.

Abstract

This paper describes a method for using interferometer measurements of downwelling thermal radiation to retrieve the properties of single-layer clouds. Cloud phase is determined from ratios of thermal emission in three "micro-windows" where absorption by water vapor is particularly small. Cloud microphysical and optical properties are retrieved from thermal emission in two micro-windows, constrained by the transmission through clouds of stratospheric ozone emission. Assuming a cloud does not approximate a blackbody, the estimated 95 % confidence retrieval errors in effective radius, visible optical depth, number concentration, and water path are, respectively, 10 %, 20 %, 38 % (55 % for ice crystals), and 16 %. Applied to data from the Atmospheric Radiation Measurement program (ARM) North Slope of Alaska – Adjacent Arctic Ocean (NSA-AAO) site near Barrow, Alaska, retrievals show general agreement with ground-based microwave radiometer measurements of liquid water path. Compared to other retrieval methods, advantages of this technique include its ability to characterize thin clouds year round, that water vapor is not a primary source of retrieval error, and that the retrievals of microphysical properties are only weakly sensitive to retrieved cloud phase. The primary limitation is the inapplicability to thicker clouds that radiate as blackbodies.

1 Introduction

Arctic clouds play significant roles in the influential, but not well understood, ice-albedo and cloud-radiation feedback mechanisms (Curry et al., 1996; Francis and Hunter, 2006). Changes in Arctic cloudiness can have discernible effects on the surface energy budget (Wang and Key, 2003; Beesley, 2000; Kay et al., 2008, 2012). Lower level Arctic stratiform clouds are regarded as an especially important target for improved numerical simulations (Smith and Kao, 1996; Harrington et al., 2000; Francis and Hunter, 2007; Fridlind et al., 2007; Klein et al., 2009; Morrison et al., 2011).

AMTD
5, 8653–8699, 2012

Observationally, the micro-structures, optical properties and thermodynamic phase of Arctic stratus have been studied previously using space-based remote sensors (Han et al., 1999; Xiong et al., 2002; Wang and Key, 2005; Tietze et al., 2011; Devasthale et al., 2011; Cesana et al., 2012) and in situ aircraft measurements (Dergach et al., 1960; Witte, 1968; Jayaweera and Ohtake, 1982; Curry et al., 2000; Rangno and Hobbs, 2001; Verlinde et al., 2007; Lampert et al., 2009; Jourdan et al., 2010; McFarquhar et al., 2011). In this paper, the focus is on retrievals of cloud microphysical properties using ground-based measurements. There are a variety of methods that can be used here, each with their respective advantages and disadvantages. One approach applied a combination of solar transmission and microwave radiometer (MWR) liquid water path to obtain cloud optical depth and effective radius, but only during the daylight months (Dong and Mace, 2003). Millimeter cloud radar (MMCR) retrievals (Shupe et al., 2005, 2006) do not have this restriction and are able to peer inside clouds. However, interpreting a radar signal is made more difficult when, as is often the case in the Arctic, large ice crystal precipitation particles are co-located with small liquid cloud particles (Hobbs et al., 2001). Lidar depolarization has been used effectively to constrain the relative contributions of ice and liquid (van Diedenhoven et al., 2009; Bourdages et al., 2009; de Boer et al., 2011; Shupe, 2011). Yet even here, a difficulty is that the back-scatter from shortwave lidar is weighted to much smaller particles than microwave radar, and lidar is attenuated much more rapidly by cloud.

A third approach is to use the infrared portion of the spectrum for remote sensing (Turner et al., 2003; Turner and Eloranta, 2008). While limited to thinner clouds, this approach is appealing because, from a climatological standpoint, it is downwelling thermal emission that plays a dominant role in the Arctic surface radiation balance (Beesley, 2000; Francis and Hunter, 2006). Retrievals are based on the part of the electromagnetic spectrum that is coupled to the physics in question.

Here, we modify and extend an infrared technique that was first developed by Mahesh et al. (2001) (hereafter M01) for retrieving the microphysical properties of Antarctic ice clouds, and is extended here to Arctic ice and liquid clouds. Cloud phase is

AMTD
5, 8653–8699, 2012

assessed using a newly developed tri-spectral scheme. The method described here is expected to be particularly accurate for three reasons. First, the remote sensing technique is anchored in two places: measurements of cloud emissivity within the atmospheric window are combined with measured cloud transmittance of 9.6-μm (1040 cm^{-1}) ozone emission. Effectively, stratospheric ozone replaces the sun in solar retrieval techniques. Second, retrievals are based on pairs of narrow spectral windows where sensitivity to water vapor is low while maintaining response to a particularly broad range of cloud properties. Third, the absorptivity of ice and liquid at 9.6 μm is almost identical, and this constrains errors in retrievals of cloud properties that might be associated with errors in cloud phase identification.

The retrieval method is outlined in Sect. 2. Section 3 describes the measurements used in this study. The error in the retrieval method is analyzed in Sect. 4. The retrieval method is evaluated in Sect. 5 and a summary is presented in Sect. 6.

2 The modified M01 retrieval algorithm

The retrieval algorithm described here is based on retrievals of a cloud particle "effective radius" (r_e) and optical depth in the geometric-optics limit at visible wavelengths (τ). Here, r_e is proportional to the ratio of the bulk ice or liquid volume to the scattering cross-section of the particle, as introduced by Hansen and Travis (1974). The definition applies equally to all shapes, independent of whether they are hexagonal ice crystals or spherical droplets.

The retrieval process has several important components. Narrow bands or "microwindows" are selected in the atmospheric window and ozone band where atmospheric water vapor emission is particularly small. It is by comparing values of measured values of cloud transmissivity and emissivity in these microwindows to theoretically estimated values that cloud phase, effective radius and optical depth are inferred. These quantities can be combined to provide cloud water path, and, in combination with estimates

AMTD
5, 8653–8699, 2012

of cloud thickness, cloud particle concentration. The full retrieval algorithm, including these modifications is illustrated in Fig. 1.

2.1 Micro-window selection

For purposes of measurement and calculation of cloud window emissivity, M01 identified micro-windows with a width of 2 cm^{-1} where water vapor absorption is particularly small and with varying sensitivity of particle absorption efficiency Q_{abs}, to particle radius. As shown in Fig. 2, candidate microwindows in the atmospheric window are centered at 830.7 (a), 862.5 (b), 903.5 (c), 917.5 (d), 935.8 (e), 960.4 (f) and 988.4 (g) cm^{-1}. The values of liquid water and ice Q_{abs} are computed from Mie theory (Wiscombe, 1980) based on their respective complex refractive indices (Warren and Brandt, 2008; Wieliczka et al., 1989). It is from this set that we determine pairs for which, as shown in Fig. 3, there is varying sensitivity of the water and ice absorption coefficient (Q_{abs}) for a range of particle radii (r) (r here, as it is applied to ice crystals, is more a radiative length scale than a spherical radius).

As shown in Fig. 3, the sensitivity of Q_{abs} to r is not the same in every microwindow. To exploit differences in size sensitivity, the retrieval method applied here uses the micro-window wavenumber pair 862.5 (b) and 935.8 cm^{-1} (e). For these wavenumbers, a look-up table is calculated for cloud emissivity ε in the two micro-windows, and cloud transmittance in the ozone band t, for various values of r_e and τ for a range of effective radii $r_e < 50$ µm and visible optical depths $\tau < 16$, using the Discrete Ordinates Radiative Transfer code (DISORT; Stamnes et al., 1988). Emissivity and transmissivity are defined by

$$\varepsilon(\nu) = I(\nu)/B(T_c, \nu) \quad (1)$$

$$t = 1 - \varepsilon \quad (2)$$

where I is the radiative intensity and $B(T_c)$ is the intensity of blackbody radiation for cloud base temperature T_c. The calculated value of $\varepsilon(\nu)$ is an "effective emissivity" that

AMTD
5, 8653–8699, 2012

implicitly incorporates the small added component from reflection, normally of order 2 % (see Turner, 2005). Calculated this way, the calculated effective emissivity is more directly comparable to ground-based measurements of downwelling $I(\nu)$, which also implicitly incorporate both thermal emission and reflection.

Figures 4 and 5 shows microwindow t (between 1038 and 1042 cm^{-1}), the aforementioned ε pairs, and their difference $\varepsilon_b - \varepsilon_e$, calculated with DISORT, as a function of r_e and τ for both liquid and ice clouds. The choice of this particular split-window has several strengths. First, the choice of ε_b and ε_e gives broad sensitivity to a wide range of values of r_e and τ for both liquid and ice clouds. For the purpose of retrievals, we can assume sensitivity for a range of parameter space bounded by a cloud transmissivity within the ozone band t that is greater than 0.05, and a cloud emissivity ε_b at 862.5 cm^{-1} that is less than 0.95 and greater than 0.05.

The second strength is that the mapping of r_e and τ for a particular value of $\varepsilon_b - \varepsilon_e$ is comparatively insensitive to whether the cloud is assumed to be liquid or ice (Fig. 5). The mapping is not perfect, but the sensitivity to phase is small compared to other micro-window combinations and it is further constrained by the incorporation of ozone band transmissivity t_{ozone} in the retrieval algorithm. The sensitivity of cloud transmissivity to assumed cloud phase is only moderately large ($\sim$ 10 %) for optically thick clouds with very small particles, clouds that in any case can normally be assigned as being liquid. The reason for the weak dependence of transmissivity on cloud phase is that the imaginary component of the refractive index at 1040 cm^{-1} is close to 0.045 for both ice and water (Warren and Brandt, 2008).

2.2 Phase determination

Remote determination of cloud phase using infrared techniques makes use of a difference in refractive index between ice and water (e.g. Strabala et al., 1994; Turner et al., 2003; King et al., 2004; Chylek et al., 2006; Riedi et al., 2007). Strictly, what is retrieved is a cloud phase that is "radiative" rather than microphysical. For example, it is common for liquid clouds in the Arctic to contain precipitating snow crystals (Hobbs

AMTD
5, 8653–8699, 2012

and Rangno, 1998; Pinto et al., 2001; McFarquhar et al., 2011). Snow crystals, while larger than droplets, are found in much lower concentrations and make a near negligible contribution to the total infrared absorption cross-section density (e.g. Fig. 7). From a radiative perspective, such clouds are purely liquid despite being microphysically "mixed-phased".

One effective approach for phase identification has been to take advantage of pronounced spectral differences between liquid and ice in the far-infrared portion of the spectrum (Turner, 2005). The disadvantage is that retrievals tend to be constrained to drier atmospheres because strong rotational-band water vapor absorption contaminates the cloud signal. Here we present in Fig. 6 a tri-spectral phase retrieval method that exploits differences in cloud emissivity within the atmospheric window, by focusing on narrow micro-windows where water vapor absorption is particularly small (Fig. 3). We have found that micro-windows at 862.5 cm^{-1} (ε_b), 935.8 cm^{-1} (ε_e) and 988.4cm^{-1} (ε_g) can be paired to neatly separate cloud phase for much of the plausible space in (r_e, τ). Figure 6 shows that a full range of plausible parameter space in r_e and τ for ice and liquids lies neatly along two distinct lines in a space of $\varepsilon_b/\varepsilon_e$ and $\varepsilon_e/\varepsilon_g$. This suggests that, roughly, where measurements of the ratio $\chi = (\varepsilon_b/\varepsilon_e)/(\varepsilon_e/\varepsilon_g)$ are greater than unity, the cloud can be identified as being liquid. The opposite is true for ice clouds. Clouds that are more spectrally flat, or in between ice and liquid, are not amenable to phase discrimination and are labelled "uncertain".

2.3 Estimation of cloud emissivity from measurements

In principle, cloud emissivity can be calculated from Eq. (1) using ground-based radiometer measurements of down-welling spectral radiance $I_{meas}(\nu)$ combined with some estimate of cloud temperature. This works, providing that there is negligible emission by atmospheric constituents between the cloud and the ground.

We have chosen micro-windows where emission and absorption of radiation by atmospheric gases is particularly small. However, cases can exist where below-cloud hydrometeors contribute non-negligibly to downwelling thermal radiance. To address this

AMTD
5, 8653–8699, 2012

possibility, we first estimate a characteristic precipitation particle radius and number concentration using a precipitation retrieval method we previously developed in Zhao and Garrett (2008). This technique retrieves precipitation microphysical properties as a function of radar reflectivity and Doppler velocity. The absorption ($Q_{\mathrm{abs,P}}(\nu)$) and extinction ($Q_{\mathrm{ext,P}}(\nu)$) coefficients for precipitation can be computed from Mie theory (Wiscombe, 1980) based on the retrieved precipitation particle radius (r) and precipitation phase. From these values, precipitation spectral emissivity ($\varepsilon_{\mathrm{P}}(\nu)$) can be determined from

$$\varepsilon_{\mathrm{P}}(\nu) = 1 - \exp\left(-\int_{\Delta z} \pi Q_{\mathrm{ext,P}}(\nu) N r^2 \mathrm{d}z\right) \tag{3}$$

where N is the precipitation particle concentration, and Δz is the depth of the precipitation layer.

For greatest precision, the below cloud contribution from water vapor contribution to downwelling radiance should also be included. In this case, the corresponding emissivity $\varepsilon_{\mathrm{v}}(\nu)$, could in principle be calculated from Eq. (1) based on measured water vapor profiles using a Line by Line Radiative Transfer Model (LBLRTM; Clough et al., 1992) based on measured ozone, temperature, and moisture profiles. Noting that transmittances multiply, the total emissivity of water vapor and precipitation $\varepsilon_{\mathrm{vP}}$ would be

$$\varepsilon_{\mathrm{vP}} = \varepsilon_{\mathrm{v}} + (1 - \varepsilon_{\mathrm{v}})\,\varepsilon_{\mathrm{P}} \tag{4}$$

in which case, ignoring the second-order term in $\varepsilon_{\mathrm{v}}\varepsilon_{\mathrm{P}}$, the corrected form of Eq. (1) for cloud emissivity is

$$\varepsilon(\nu) = \frac{I_{\mathrm{meas}}(\nu) - \varepsilon_{\mathrm{vP}}(\nu)\,B(T_{\mathrm{P}}, \nu)}{(1 - \varepsilon_{\mathrm{vP}})\,B(T_{\mathrm{C}}, \nu)} \tag{5}$$

where $I_{\mathrm{meas}}(\nu)$ is the surface measured radiation at wavenumber ν, and $B(T_{\mathrm{P}}, \nu)$ and $B(T_{\mathrm{C}}, \nu)$ represent blackbody radiation at ν for mean precipitation and cloud temperature T_{P} and T_{C}; temperatures are estimated by matching detected heights to measured

AMTD
5, 8653–8699, 2012

atmospheric temperature soundings. Here, for the sake of retrieval simplicity we make the approximation that $\varepsilon_{vP} \simeq \varepsilon_P$. The associated error from making this approximation is discussed in Sect. 5.2.

With the contribution of precipitation to thermal emission excluded, the contribution of clouds and other trace gases to downwelling surface radiance is

$$I_C(\nu) = \varepsilon(\nu) B(T_C, \nu) \tag{6}$$

Figure 7 shows values of ε_P obtained near Barrow, Alaska based on precipitation properties derived by Zhao and Garrett (2008). Retrieved values of ε_P range from 0 to 0.14 with lower and upper quartile values of 0.01 and 0.04, respectively. Because values of ε_P are generally low, the combined contribution of water vapor and precipitation to I_c is typically about 1 %, in which case it can usually be ignored for the purpose of retrieving cloud properties. However, in the upper quartile, precipitation has a thermal emissivity greater than 0.05, and contributes in excess of 3 % to I_{sky}. Therefore, if a higher certainty of accuracy is desired, thermally based cloud retrievals should systematically account for the radiation contribution from both precipitation and water vapor.

2.4 Measurement of cloud transmissivity

The procedure for estimating cloud transmissivity is illustrated in Fig. 8. Estimates of cloud transmissivity within a 1038 cm^{-1} to 1042 cm^{-1} microwindow in the ozone band follow a series of steps. First, surface radiance measurements $I_{meas}(\nu)$ are corrected for precipitation emission to give

$$I_{sky}(\nu) = I_{meas}(\nu) - \varepsilon_P(\nu) B(T_P, \nu) \tag{7}$$

Then, from the relation $I_{sky}(\nu) = B(T_{cb}, \nu)$, an atmospheric brightness temperature T_{cb}, representative of cloud base, is evaluated between 960 cm^{-1} and 975 cm^{-1} and between 1070 cm^{-1} and 1085 cm^{-1}, just outside the P and R branches of ozone emission.

AMTD
5, 8653–8699, 2012

Second, using linear interpolation, the value of T_{cb} is evaluated within the P and R branches. From this value, the background radiance from all sources other than ozone and precipitation, $I_{bkg}(\nu)$, is inferred.

Finally, to calculate cloud transmittance t of P and R branch ozone emission. To do this, I_{bkg} is subtracted from I_{sky} and the difference then divided by calculated values of the clear sky radiance I_{clear} without precipitation or clouds

$$t(\nu) = I_{cloudy}(\nu)/I_{clear}(\nu) = (I_{sky}(\nu) - I_{bkg}(\nu))/I_{clear}(\nu) \quad (8)$$

where I_{clear} is estimated using the LBLRTM based on measured atmospheric ozone, temperature and moisture profiles. Values of t between two ranges – 1020 cm^{-1} to 1040 cm^{-1} in the P branch and 1048 cm^{-1} to 1065 cm^{-1} in the R branch – are used to interpolate values of t in the Q branch between 1040 cm^{-1} and 1048 cm^{-1}. Values of t within the desired microwindow between 1038 cm^{-1} and 1042 cm^{-1} are a subset of these calculated transmittance values.

2.5 Cloud properties

Cloud effective radius (r_e) and visible optical depth (τ) can now be obtained in a two step process. First observed values of ε_b, ε_e and ε_g are calculated from measured downwelling radiances, corrected for below cloud atmospheric emission. These are then used to identify cloud phase using the described tri-spectral retrieval method.

Then, the observed values of ε_b and ε_e, along with observed values of t in the ozone band microwindow, are compared to those in a look-up table for r_e and τ for either ice or liquid clouds, or in the case of mixed-phased clouds, both. Calculations are a simple minimization of

$$[\varepsilon_b, \Delta\varepsilon, t]_{observations} - [\varepsilon_b, \Delta\varepsilon, t]_{calculations} \quad (9)$$

where, $\Delta\varepsilon = \varepsilon_b - \varepsilon_e$.

The variables in the minimization algorithm are weighted according to the relative magnitudes of their uncertainties. Uncertainties in ε result mostly from uncertainties

AMTD
5, 8653–8699, 2012

in estimates of cloud-base temperature and uncertainties in measurements of downwelling spectral radiance, due for example to water vapor emission. In the latter case, these uncertainties are expected to manifest themselves as a bias. Values of $\Delta\varepsilon$, on the other hand, are highly robust to errors in temperature estimates, so they are weighted five times higher than emissivity ε_b. Cloud transmittance (t) is weighted three times higher than ε_b because it is comparatively insensitive to uncertainties in estimated cloud phase. No cloud property retrievals are made for clouds with an uncertain phase. However, for mixed-phased clouds, cloud properties are a simple average of the estimates of r_e and τ for assumed liquid and ice clouds.

By assuming a log-normal cloud particle size distribution, such cloud properties as water path WP and particle number concentration N, are related to retrieved r_e and τ through

$$\mathrm{WP} = 2\rho r_e \tau / 3 \tag{10}$$

$$N = 3\exp(3\sigma^2)\mathrm{WP}/(4\pi\rho r_e^3 \Delta H) \tag{11}$$

where ρ is the water or ice density depending on the phase, σ the assumed standard log-normal deviation of the droplet size distribution, and $\Delta H = H_{top} - H_{base}$ is the difference between the measured cloud-top and -base heights.

We estimate a suitable value for σ of 0.32 ± 0.10 based on a reanalysis of airborne measurements of droplet size distributions $< 50\,\mu m$ diameter obtained during four University of Washington field campaigns in the Arctic between 1982 and 1998 (Garrett et al., 2004). It is more difficult to obtain a representative value for ice clouds, in part due to concerns about aircraft instrument performance (Field et al., 2003), but the value of σ is not necessarily markedly different (e.g. Rangno and Hobbs, 2001, Fig. 8). Accordingly, σ for ice and liquid are assumed to be identical, but with an uncertainty for ice that is twice as large, i.e. $\sigma = 0.32 \pm 0.20$.

Generally it is accepted that saturation effects limit infrared retrieval techniques to values of WP lower than about $40\,g\,m^{-2}$ (Garrett et al., 2002). But this is not always the case. The imaginary component of the refractive index is 0.046 for both ice and

AMTD
5, 8653–8699, 2012

water in the portion of the ozone transmission band between 1038 cm^{-1} and 1042 cm^{-1} (Wieliczka et al., 1989). Therefore, in a bulk water medium, an ozone band transmittance value of 0.05 – the sensitivity cutoff for t in the infrared retrieval technique used here – should correspond to a liquid water absorption path of 60 $g\,m^{-2}$. The absorption path able to be detected can even be larger than 60 $g\,m^{-2}$ if cloud particle radii are larger than about 10 µm (Fig. 4): a portion of particle mass lies within the particle interior where it is effectively invisible to the incident infrared radiation; thus, radiative absorption is focused within a skin depth smaller than the droplet radius itself, and only a fraction of condensed mass absorbs incident radiation.

3 Measurements

The datasets used in this study are from the DOE Atmospheric Radiation Measurement Program (ARM) Program North Slope of Alaska – Adjacent Arctic Ocean (NSA-AAO) site, the NOAA Global Monitoring Division (GMD), the European Remote Sensing satellite (ERS) Global Ozone Monitoring Experiment (GOME), and the National Weather Service (NWS). The period of data acquisition is 2000 to 2003, to be consistent with analysis described in Garrett and Zhao (2006). All ground-based data used here were obtained near Barrow, Alaska. Table 1 summarizes the measurement site, instruments, resolution, and accuracy.

3.1 Cloud remote sensing measurements

Cloud properties were measured using a combination of active and passive remote sensors. Key instruments used for cloud retrievals from NSA-AAO include the Vaisala 25 K Laser Ceilometer, the Micropulse Lidar, the Atmospheric Emitted Radiance Interferometer (AERI), and the millimeter wavelength cloud radar (MMCR) (Peppler et al., 2008).

AMTD
5, 8653–8699, 2012

The Atmospheric Emitted Radiance Interferometer (AERI) is an automated ground-based passive interferometer, which measures downwelling atmospheric radiance spectra within a 1.3° field of view. The spectral range the AERI covers is between 400 and 3300 cm^{-1} with a spectral resolution of approximately 1 cm^{-1}. The radiometric accuracy of AERI instruments (for 3 standard deviations) is better than 1 % of ambient radiance (Knuteson et al., 2004). For the atmospheric window measurements used here to detect cold arctic clouds this corresponds to uncertainties better than 0.5 $mW(m^2 sr cm^{-1})^{-1}$.

A Vaisala Laser Ceilometer is used to determine cloud base with an uncertainty of 7.6 m (Dong et al., 2005). Since its accuracy diminishes with height (Jay Mace, personal communication, 2011), retrievals are restricted here to clouds with bases less than 4000 m altitude. The micropulse lidar provides clouds boundaries with a height resolution of 30 m (Campbell et al., 2002). The Millimeter-wave Cloud Radar (MMCR) provides profiles of radar reflectivity with measurement uncertainties of 0.5 dB. MMCR estimates of cloud boundaries have an accuracy of 45 m (Dong and Mace, 2003). Here they are used to detect cloud top as well as to exclude cases with multiple cloud layers (for example cirrus over stratus). More complicated scenes with multi-layered liquid clouds and ice crystal precipitation filling the vertical space between layers are interpreted as single layer clouds.

We found that the ceilometer occasionally detects the base of a thin cloud that is invisible to the radar; or, if the cloud precipitates, the radar cloud top lies below the ceilometer cloud base. When this occurs, retrievals of cloud thickness, and hence number concentration N are impossible or nonsensical. However, estimates of other cloud properties are still performed since they do not rely on cloud thickness measurements.

For the purpose of a later comparison with the proposed thermal retrieval method, values of column-integrated liquid water path (LWP) are derived from brightness temperatures measured with a microwave radiometer (MWR) (Liljegren et al., 2001). The root-mean-square uncertainties of the LWP retrievals are commonly between 10 $g m^{-2}$ and 15 $g m^{-2}$, but can be higher than 30 $g m^{-2}$ (Marchand et al., 2003).

AMTD
5, 8653–8699, 2012

3.2 Atmospheric ozone, temperature, and moisture

Calculation of cloudy transmission t of ozone emission requires profiles of atmospheric ozone, temperature and moisture. Surface ozone concentrations are provided from ultraviolet ozone photometers at the GMD site at Barrow, Alaska, and stratospheric ozone profiles (> 6 km) are provided by ERS-GOME. Ozone profiles from the surface to 6 km are obtained by interpolating between GOME stratospheric ozone profiles (Burrows et al., 1999) and GMD surface ozone measurements. The interpolation process uses a standard seasonal ozone profile to weight interpolated ozone profiles between the surface and 6 km height. The time resolution for ozone profile measurements is 6 h and hourly at the surface. The accuracy of satellite measured profiles of stratospheric ozone concentration is about 5–10 % (∼ 100 ppb) (Lapaolo et al., 2007), and the accuracy of surface ozone concentration measurements from GMD is about 2 %.

Temperature and moisture profiles are obtained from twice-daily NWS balloon-borne profiles up to the maximum measured altitude - typically about 16 km. Above that level, European Center for Medium range Weather Forecasting (ECMWF) ERA-40 reanalyses are used (Uppala et al., 2005). Above 60 km, temperatures and humidities are fixed to 230 K and 5 ppmv. For times intermediate to the NWS profile intervals, a temporal linear interpolation is applied to the data. For heights intermediate to measured profile levels, cloud base and cloud top temperatures are obtained by applying a vertical linear interpolation. For the purpose of retrievals, we assume that balloon-sonde tropospheric water vapor measurements have an uncertainty of 15 % is assumed and that the measured upper-level temperature profiles have an uncertainty of 5 %, or roughly ±12 K.

In the troposphere, profiles are important for assessing cloud temperature. Based on observed temperature variability during the diurnal cycle, uncertainties in cloud base and cloud top temperatures are estimated to be ±3 K. Other trace gases, such as carbon dioxide (CO_2) and methane (CH_4) do not have primary absorption bands at the

AMTD
5, 8653–8699, 2012

frequencies used here. Associated uncertainties are less than 1 % and not considered in detail.

4 Error analysis

Sources of uncertainty in retrievals come from both the measurements and the retrieval technique itself. To calculate the magnitude of the errors that are specific to the retrieval technique, the technique is tested on synthetically created clouds. These errors are then combined with errors in the technique associated with measurement uncertainties. The intent here is to evaluate the extent to which adequate physics was implemented correctly in the algorithm development.

We test the ability of the retrieval technique to accurately infer synthetically specified values of cloud properties. Downwelling spectral radiance (I) at the surface is calculated using DISORT based on synthetically specified values of r_e, τ, H_{base}, H_{top} and cloud temperature. From the values of I, the cloud properties r_e and τ are "retrieved" and compared with the synthetic values.

In this test, specified values of τ and r_e range from 0.1 to 16.0, and from 3.0 µm to 50.0 µm, respectively. Cloud base and cloud top height and temperature are set to 223 m and 438 m, and 260 K and 256 K, respectively. Ozone (O_3), temperature (T), and water vapor (WV) profiles (O_3 and T profiles are shown in Fig. 9), are subjectively chosen from measurements at ARM NSA-AAO obtained on 7 May 2000 and 15 January 2001.

Figure 10 shows that "retrieved" cloud properties agree very well with the synthetic values. Errors associated with retrievals of τ are not shown since they are < 2 % throughout the parameter space in r_e and τ. For r_e, LWP, and N, computed values of 95 % confidence retrieval errors associated with the method exceed 10 % only where values of r_e exceed 30 µm and values of τ exceed about 6, presumably because Q_{abs} is only a weak function of r_e and the sensitivity of cloud emissivity to τ decreases as a cloud thickens to approximate a blackbody. That we have assumed clouds that

AMTD
5, 8653–8699, 2012

are microphysically homogeneous in the vertical may mean that additional errors are associated with true clouds.

The primary uncertainties in the retrievals arise from measurement errors. Based on the discussion of measurement accuracies in Sect. 4, the 95 % confidence uncertainties in cloud base temperature (T_c), AERI radiance (I), water vapor profile (H_2O), ozone profile (O_3), and cloud depth (ΔH) are estimated to be about ±3 K, 0.5 mW$(m^2\,sr\,cm^{-1})^{-1}$, 15 %, 100 ppb, and 50 m, respectively. Uncertainties in stratospheric temperature and moisture profiles are 5 %. Aircraft measurements from the FIRE-ACE field campaigns show uncertainty in the cloud particle log-normal distribution spectral width (σ) to be ±0.10 for liquid clouds (Garrett et al., 2004), and it is assumed to be ±0.20 for ice clouds.

Assuming that errors from measurements of T_c, I, O_3, ΔH and σ are independent, the 1-sigma retrieval error in property x due to combined measurement and retrieval method errors is

$$\sigma_x^2 = \sigma_M^2\left(\frac{\partial x}{\partial M}\right)^2 + \sigma_I^2\left(\frac{\partial x}{\partial I}\right)^2 + \sigma_{H_2O}^2\left(\frac{\partial x}{\partial H_2O}\right)^2 + \sigma_{O_3}^2\left(\frac{\partial x}{\partial O_3}\right)^2 + \sigma_T^2\left(\frac{\partial x}{\partial T}\right)^2 + \sigma_{\Delta h}^2\left(\frac{\partial x}{\partial \Delta H}\right)^2 + \sigma_\sigma^2\left(\frac{\partial x}{\partial \sigma}\right)^2 \quad (12)$$

where σ_y is the standard deviation of variable y, M represents the retrieval method, and I, H_2O, O_3, T, ΔH and σ are measurement variables, the brackets () contain the sensitivity of x to the measurements or retrieval method. Here, the covariance between the different quantities is assumed to be zero.

Table 2 shows estimates of the liquid and ice cloud retrieval errors due to combined uncertainties in the retrieval method and measurements. The errors in r_e, τ, and WP are due mainly to uncertainties in cloud base temperature and AERI radiance. Errors in N are also strongly dependent on uncertainties in cloud depth and the standard deviation of the droplet or ice size distribution. The combined 95 % confidence uncertainties in cloud r_e, τ, and WP are about 10 %, 20 %, and 16 %. For N, they are and 38 % and 55 % for ice and liquid, respectively.

AMTD
5, 8653–8699, 2012

5 Evaluation

5.1 Comparison with measurements

Using the phase identification method employed here, it was possible to identify whether the cloud phase was liquid or ice in 65 % of cases where there were thin clouds with $0.05 < \varepsilon_b < 0.95$. The remainder of cases were classified as having uncertain phase. One way to assess the magnitude of error in the cloud phase determination is to examine the detected phase above and below certain known phase transitions, such as the melting and homogeneous freezing points. For thin cloud cases with cloud base temperatures higher than 273 K, clouds were classified as being ice in 6 % of cases and liquid in 45 % of cases. The respective numbers for clouds with base temperatures below 238 K were 73 % and 11 %. These numbers suggest that, in about 15 % of cases where a phase identification was made, the phase was misclassified.

A second approach for evaluating the phase retrievals is to compare with ARM Microwave Radiometer (MWR) measurements. The MWR is insensitive to ice so, in principle, it should not detect water when the infrared method identifies an ice cloud. Figure 11 shows a comparison between retrieved values of LWP and IWP using the infrared-based method and the LWP derived from the MWR. What is shown is a fairly high correlation ($r^2 = 0.46$) between microwave and thermal IR retrievals of LWP, but with a 10 g m^{-2} to 15 g m^{-2} positive bias in the MWR LWP measurements, consistent with known uncertainties in the MWR retrievals (Marchand et al., 2003). Thermal retrievals of IWP and the MWR LWP do not correlate well ($r^2 = 0.06$). When the infrared based retrievals of IWP are non-zero, the MWR LWP retrievals are consistently within MWR uncertainty bounds.

For those cases where the retrieved cloud phase is "uncertain", it may nonetheless be possible to retrieve cloud optical depth τ and effective radius r_e to within an acceptable degree of confidence. Figure 12 shows a comparison between the values of retrieved τ and r_e for "uncertain" cases depending on whether the cloud optical properties are treated as being either liquid or ice. For example, if the cloud were composed

AMTD
5, 8653–8699, 2012

of ice, but the cloud microphysics were calculated as if it were liquid, then the optical depth would be overestimated, and the effective radius would be underestimated, by about 15 %. These uncertainties are comparable to those due to measurement errors where the cloud phase has been correctly determined (Table. 2).

5.2 Sensitivity to water vapor

For the emissivity measurement calculations described here, the contribution of water vapor to the measured signal is not subtracted (Eq. 6) because its contribution is, for the most part, negligible. Estimated retrieval uncertainties associated with water vapor were estimated to be within 1 % for τ, r_e and WP.

For comparison, a prior study by Turner (2005) described the "MIXCRA" algorithm, which, while highly flexible and accurate in its application of AERI measurements to Arctic cloud retrievals (Turner and Eloranta, 2008), was nonetheless constrained to scenes with precipitable water vapor (PWV) amounts less than 1 cm. This precondition could be removed, but only if the cloud phase was known a priori, as it was only the phase identification component of MIXCRA that involved frequencies outside the atmospheric window.

By contrast, the retrievals described here, including those of phase, are based only on measurements within the atmospheric window where water lacks single-molecule rotational or vibrational fundamental modes. The disadvantage of this approach is that differences in the absorption properties of ice and liquid clouds are not always clearly separated. Also, water vapor continuum absorption does remain in the window. Nonetheless, water vapor emission is implicitly factored into the retrievals through comparisons of transmissivity inside and just outside the 1040 cm^{-1} ozone band that are used to calculate cloud transmissivity (Fig. 8). Moreover, cloud emissivity estimates are evaluated within "microwindows" where atmospheric absorption and emission by water vapor is particularly small.

Figure 13, shows the influence of water vapor on the retrievals of r_e. Not subtracting water vapor in estimates of cloud emissivity causes differences in retrieved values of

AMTD
5, 8653–8699, 2012

r_e. In 86 % of cases the difference is less than 0.01 µm, which is the precision of the retrieval technique. In the remainder of cases the difference is generally still very small, in the vicinity of 1 to 2 percent. In only a very few cases is the difference in excess of 10 %, although still less than 1 µm.

What is interesting is that cases with relatively high errors are usually, but not necessarily associated with high values of PWV. More important than the absolute value of PWV is the relative contributions of water vapor and cloud to downwelling radiance. Naturally, these two quantities tend to covary with temperature. Drier conditions may be associated with lower water vapor emission, but they are also associated with thinner, less strongly emitting clouds. In this case, the contribution of water vapor to the measured signal may be much larger than is typical, if still small.

5.3 Case study

Figure 14 shows lidar and radar imagery from NSA-AAO for a scene on 13 January 2001 that is both complex while not being unusual. The day is characterized by two cloud layers: a high layer above 4 km altitude that resembles cirrus fallstreaks, and a lower thin cloud layer at around 1 km altitude with precipitation falling beneath.

Figure 15 shows retrieved properties for this case. What is observed is a high cirrus cloud in the beginnings of the day that, with some overlap, transitions to a thin low-level cloud. Because the cirrus and lower-level cloud are well separated, cloud retrievals are made here even though the day is largely multi-layered. With a few exceptions, when cloud phase is explicitly retrieved, it indicates that the cirrus cloud is ice and the low-level cloud is liquid. The spectral slope $\chi = \left(\varepsilon_b/\varepsilon_e\right) / \left(\varepsilon_e/\varepsilon_g\right)$ used in part to characterize cloud phase is relatively consistent within each of these two regions: the low-level cloud has median and [lower, upper] quartile values of χ are 1.04 [1.03 1.05] versus 0.90 [0.85 0.93] in the cirrus.

Median and [lower, upper] quartile values for the low-level liquid cloud properties are a thickness of 250 [236 272] m, an emissivity of 0.90 [0.83 0.93], a visible optical depth of 6.1 [5.1 7.2], a droplet effective radius of 4.7 [3.8 6.2] µm, droplet concentrations

AMTD
5, 8653–8699, 2012

of 192 [130 434] cm^{-3}, and a liquid water path of 22 [15 25] $g\,m^{-2}$. For the ice crystal cirrus, median and [lower, upper] quartile values are a thickness of 589 [237 930] m, an emissivity of 0.09 [0.07 0.16], a visible optical depth of 0.20 [0.16 0.35], an ice crystal effective radius of 48 [39 49] µm, ice crystal concentrations of 69 [47 128] l^{-1}, and a liquid water path of 6.1 [4.9 8.0] $g\,m^{-2}$.

5.4 Seasonal variability

Figure 16 shows the retrieved seasonable variability in cloud properties at NSA-AAO between 2000 and 2003, presented as monthly means. Cloud cover statistics are presented for both all clouds and those graybody clouds with $\varepsilon_b < 0.95$. The remainder of parameters shown apply only to graybody clouds for which the thermal IR retrieval technique presented here applies. Therefore, the statistics do not represent a true climatology since they omit thicker clouds that radiate as blackbodies.

In general, the statistics are qualitatively consistent with prior studies into the seasonality of Arctic clouds (e.g. Shupe et al., 2005; Kay and Gettelman, 2009; Devasthale et al., 2011). The Arctic is cloudy. Thin graybody clouds are a substantial fraction of the total, and on average, these clouds are found at low levels with bases below 2 km altitude. In summer, when conditions are warmer, the first cloud layer viewed from the ground is rarely ice. Also in summer, liquid clouds have a higher water path and are more optically thick. When ice clouds are present, they have crystal concentrations that are about two orders of magnitude lower than liquid droplet concentrations, and effective radii that are about four times as large. The optical depth and effective radii of all gray-body clouds are intermediate to those of the liquid and ice clouds, but on average they are most closely approximated by the liquid cloud portion.

AMTD
5, 8653–8699, 2012

6 Conclusions

A method has been developed for the retrieval of Arctic cloud microphysical and macrophysical properties based on cloudy thermal emission and stratospheric ozone cloudy thermal transmission. For both liquid and ice clouds, two emissivity micro-windows are selected in the atmospheric window based on the sensitivity of the particle absorption coefficient to particle effective radius r_e. Cloud micro-structure properties are obtained by matching estimates of cloud emissivity and transmissivity from measurements with calculated values from a look-up table. The retrieval technique is limited to graybody clouds with cloud optical depths τ less than 16 and cloud particle effective radii r_e smaller than 50 µm.

Cloud phase is determined from the ratios of three emissivity micro-windows within the atmospheric window. These can be paired to neatly separate cloud phase for much of the plausible space in (r_e, τ). The phase retrieval reflects the radiative properties of the clouds: mixed-phased clouds might be identified as being liquid if the ice crystals contribute negligibly to their thermal emission.

Error analysis indicates that the method's main sources of retrieval error come from uncertainties in measured cloud base temperature, surface thermal radiance, and the stratospheric ozone profile. Because retrievals are constrained by both cloud transmittance and emissivity, they display very low sensitivity to water vapor. The respective 95 % confidence retrieval errors in r_e, τ, WP, and N are about 10 %, 20 %, 16 % and 38 % for liquid cloud, and about 10 %, 20 %, 16 % and 55 % for ice clouds. The retrievals of cloud microphysical properties require an a priori determination of clouds phase. Where phase cannot be determined, or is in error, the bias in retrievals of r_e and τ is approximately 15 %.

The thermal IR based method described here is particularly well suited to optically thin clouds that can be difficult to characterize using other remote sensing approaches. For example, the average liquid water path retrieved by the microwave radiometer (MWR) between the months of November and February is 28 g m^{-2}. Such clouds are

AMTD
5, 8653–8699, 2012

optically thin in the thermal IR, but they lie within the MWR retrieval noise. Also, retrievals methods based on solar transmission can be well suited for describing cloud properties in the summer (e.g. Dong and Mace, 2003), but they are inapplicable during the winter night. By contrast, thermal emission is year round. The primary limitation of the thermal IR approach discussed here is that it requires that clouds cannot approximate blackbodies. Clouds tend to be most optically thick in summer when this method could be used in combination with other approaches.

Acknowledgement. This work was supported by the National Science Foundation through grants 0303962 and 0649570, the Clean Air Task Force, and through NOAA by grant 2308014. We are grateful to P. V. Hobbs for having provided aircraft data from FIRE-ACE and Jay Mace and Sally Benson for plots of the lidar and radar signals.

References

Beesley, J. A.: Estimating the effect of clouds on the arctic surface energy budget, J. Geophys. Res., 105, 10103–10117, 2000. 8654, 8655

Bourdages, L., Duck, T. J., Lesins, G., Drummond, J. R., and Eloranta, E. W.: Physical properties of High Arctic tropospheric particles during winter, Atmos. Chem. Phys., 9, 6881–6897, doi:10.5194/acp-9-6881-2009, 2009. 8655

Burrows, J. P., Weber, M., Buchwitz, M., Rozanov, V., Ladstätter-Weißenmayer, R., A. DeBeek, R., Hoogen, R., Bramstedt, K., Eichmann, K.-U., and Eisinger, M.: The Global Ozone Monitoring Experiment (GOME) mission concept and first scientific results, J. Atmos. Sci., 56, 151–175, 1999. 8666

Campbell, J. R., Hlavka, D. L., Welton, E. J., Flynn, C. J., Turner, D. D., Spinhirne, J. D., and Scott, V. S.: Full-time eye-safe cloud and aerosol lidar observation at atmospheric radiation measurement program sites: instruments and data processing, J. Atmos. Ocean. Tech., 19, 431–442, 2002. 8665

Cesana, G., Kay, J. E., Chepfer, H., English, J. M., and de Boer, G.: Ubiquitous low-level liquid-containing arctic clouds: new observations and climate model constraints from calipso-goccp, Geophys. Res. Lett., 39, L20804, doi:10.1029/2012GL053385, 2012. 8655

AMTD

5, 8653–8699, 2012

Chylek, P., Robinson, S., Dubey, M. K., King, M. D., Fu, Q., and Clodius, W. B.: Comparison of near-infrared and thermal infrared cloud phase detections, J. Geophys. Res., 111, D20203, doi:10.1029/2006JD007140, 2006. 8658

Clough, S. A., Iacono, M. J., and Moncet, J. L.: Line-by-line calculations of atmospheric fluxes and cooling rates: application to water vapor, J. Geophys. Res., 97, 15761–15785, 1992. 8660

Curry, J. A., Rossow, W. B., Randall, D., and Schramm, J. L.: Overview of Arctic cloud and radiation characteristics, J. Climate, 9, 1731–1764, 1996. 8654

Curry, J. A., Hobbs, P. V., King, M. D., Randall, D. A., Minnis, P., Isaac, G. A., Pinto, J. O., Uttal, T., Bucholtz, A., Cripe, D. G., Gerber, H., Fairall, C. W., Garrett, T. J., Hudson, J., Intrieri, J. M., Jakob, C., Jensen, T., Lawson, P., Marcotte, D., Nguyen, L., Pilewskie, P., Rangno, A., Rogers, D. C., Strawbridge, K. B., Valero, F. P. J., Williams, A. G., and Wylie, D.: FIRE Arctic clouds experiment, Bull. Amer. Meteor. Soc., 81, 5–29, 2000. 8655

de Boer, G., Collins, W. D., Menon, S., and Long, C. N.: Using surface remote sensors to derive radiative characteristics of mixed-phase clouds: an example from M-PACE, Atmos. Chem. Phys., 11, 11937–11949, doi:10.5194/acp-11-11937-2011, 2011. 8655

Dergach, A. L., Zabrodsky, G. M., and Morachevsky, V. G.: The results of a complex investigation of the type St-Sc clouds and fogs in the Arctic, Bull. Acad. Sci. USSR, Geophys. Ser., 1, 66–70, 1960. 8655

Devasthale, A., Tjernström, M., Karlsson, K.-G., Thomas, M. A., Jones, C., Sedlar, J., and Omar, A. H.: The vertical distribution of thin features over the Arctic analysed from CALIPSO observations part I: optically thin clouds, Tellus B, 63, 77–85, doi:10.1111/j.1600-0889.2010.00516.x, 2011. 8655, 8672

Dong, X. and Mace, G. G.: Arctic stratus cloud properties and radiative forcing derived from ground-based data collected at Barrow, Alaska, J. Climate, 16, 445–461, 2003. 8655, 8665, 8674

Dong, X., Minnis, P., and Xi, B.: A climatology of midlatitude continental clouds from the ARM SGP central facility: part I: low-level cloud macrophysical, microphysical, and radiative properties, J. Climate, 18, 1391–1410, 2005. 8665

Field, P. R., Wood, R., Brown, R. A., Kaye, P. H., Hirst, E., Greenway, R., and Smith, J. A.: Ice particle interarrival times measured with a fast FSSP, J. Atmos. Ocean. Technol., 20, 249–261, 2003. 8663

AMTD
5, 8653–8699, 2012

Francis, J. A. and Hunter, E.: New insight into the disappearing Arctic sea ice, Eos Trans. AGU, 87509–87511, doi:10.1029/2006EO460001, 2006. 8654, 8655
Francis, J. A. and Hunter, E.: Changes in the fabric of the Arctic's greenhouse blanket, Env. Res. Lett., 2, 045011–+, doi:10.1088/1748-9326/2/4/045011, 2007. 8654
Fridlind, A. M., Ackerman, A. S., McFarquhar, G., Zhang, G., Poellot, M. R., DeMott, P. J., Prenni, A. J., and Heymsfield, A. J.: Ice properties of single-layer stratocumulus during the mixed-phase Arctic cloud experiment: 2. Model results, J. Geophys. Res., 112, D24202, doi:10.1029/2007JD008646, 2007. 8654
Garrett, T. J. and Zhao, C.: Increased Arctic cloud longwave emissivity associated with pollution from mid-latitudes, Nature, 440, 787–789, doi:10.1038/nature04636, 2006. 8664
Garrett, T. J., Radke, L. F., and Hobbs, P. V.: Aerosol effects on the cloud emissivity and surface longwave heating in the Arctic, J. Atmos. Sci., 59, 769–778, 2002. 8663
Garrett, T. J., Zhao, C., Dong, X., Mace, G. G., and Hobbs, P. V.: Effects of varying aerosol regimes on low-level Arctic stratus, Geophys. Res. Lett., 31, 17105–17109, 2004. 8663, 8668
Han, W., Stamnes, K., and Lubin, D.: Retrieval of surface and cloud properties in the Arctic from NOAA AVHRR measurements, J. Appl. Meteorol., 38, 989–1012, 1999. 8655
Hansen, J. E. and Travis, L. D.: Light scattering in planetary atmospheres, Space Sci. Rev., 16, 527–610, 1974. 8656
Harrington, J. Y., Feingold, G., and Cotton, W. R.: Radiative impacts on the growth of a population of drops within simulated summertime Arctic stratus, J. Atmos. Sci., 57, 766–785, 2000. 8654
Hobbs, P. V. and Rangno, A. L.: Microstructure of low and middle-level clouds over the beaufort sea, Q. J. R. Meteorol. Soc., 124, 2035–2071, 1998. 8658
Hobbs, P. V., Rangno, A. L., Shupe, M., and Uttal, T.: Airborne studies of cloud structures over the Arctic ocean comparisons with retrievals from ship-based remote sensing measurements, J. Geophys. Res., 106, 15029–15044, 2001. 8655
Jayaweera, K. O. L. F. and Ohtake, T.: Concentration of ice crystals in Arctic stratus clouds, Geophys. Res. Lett., 9, 94–97, 1982. 8655
Jourdan, O., Mioche, G., Garrett, T. J, Schwarzenböck, A., Vidot, J., Xie, Y., Shcherbakov, V., Yang, P., and Gayet, J.-F.: Coupling of the microphysical and optical properties of an Arctic nimbostratus cloud during the ASTAR 2004 experiment: implications for light-scattering modeling, J. Geophys. Res., 115, D23206, doi:10.1029/2010JD014016, 2010. 8655

AMTD
5, 8653–8699, 2012

Kay, J. E. and Gettelman, A.: Cloud influence on and response to seasonal Arctic sea ice loss, J. Geophys. Res., 114, D18204, doi:10.1029/2009JD011773, 2009. 8672

Kay, J. E., L'Ecuyer, T., Gettelman, A., Stephens, G., and O'Dell, C.: The contribution of cloud and radiation anomalies to the 2007 Arctic sea ice extent minimum, Geophys. Res. Lett., 35, L08503, doi:10.1029/2008GL033451, 2008. 8654

Kay, J. E., Holland, M. M., Bitz, C. M., Blanchard-Wrigglesworth, E., Gettelman, A., Conley, A., and Bailey, D.: The influence of local feedbacks and northward heat transport on the equilibrium arctic climate response to increased greenhouse gas forcing, J. Climate, 25, 5433–5450, doi:10.1175/JCLI-D-11-00622.1, 2012. 8654

King, M. D., Platnick, S., Yang, P., Arnold, G. T., Gray, M. A., Riedi, J. C., Ackerman, S. A., and Liou, K. N.: Remote sensing of liquid water and ice cloud optical thickness and effective radius in the Arctic: application of airborne multispectral MAS data, J. Atmos. Ocean. Tech., 21, 857–875, 2004. 8658

Klein, S. A., McCoy, R. B., Morrison, H., Ackerman, A. S., Avramov, A., de Boer, G., Chen, M., Cole, J. N. S., Del Genio, A. D., Falk, M., Foster, M. J., Fridlind, A., Golaz, J.-C., and Hashino, T., Harrington, J. Y., Hoose, C., Khairoutdinov, M. F., Larson, V. E., Liu, X., and Luo, Y., McFarquhar, G. M., Menon, S., Neggers, R. A. J., Park, S., Poellot, M. R., Schmidt, J. M., Sednev, I., Shipway, B. J., Shupe, M. D., Spangenberg, D. A., Sud, Y. C., Turner, D. D., Veron, D. E., von Salzen, K., Walker, G. K., Wang, Z., Wolf, A. B., Xie, S., Xu, K.-M., Yang, F., and Zhang, G.: Intercomparison of model simulations of mixed-phase clouds observed during the ARM mixed-phase Arctic cloud experiment. I: single-layer cloud, Q. J. Roy. Meteorol. Soc., 135, 979–1002, doi:10.1002/qj.416, 2009. 8654

Knuteson, R. O., Revercomb, H. E., Best, F. A., Ciganovich, N. C., Dedecker, R. G., Dirkx, T. P., Ellington, S. C., Feltz, W. F., Garcia, R. K., Howell, H. B., Smith, W. L., Short, J. F., and Tobin, D. C.: Atmospheric emitted radiance interferometer. Part I: instrument design, J. Atmos. Ocean. Technol., 21, 1763–1776, 2004. 8665

Lampert, A., Ehrlich, A., Dörnbrack, A., Jourdan, O., Gayet, J.-F., Mioche, G., Shcherbakov, V., Ritter, C., and Wendisch, M.: Microphysical and radiative characterization of a subvisible midlevel Arctic ice cloud by airborne observations – a case study, Atmos. Chem. Phys., 9, 2647–2661, doi:10.5194/acp-9-2647-2009, 2009. 8655

Lapaolo, M., Godin-Beekmann, S., Del Frate, F., Casadio, S., Petitdidier, M., McDermid, I. S., Leblanc, T., Swart, D., Meijer, Y., Hansen, G., and Stebel, K.: GOME ozone profiles retrieved

AMTD
5, 8653–8699, 2012

by neural network techniques: a global validation with lidar measurements, J. Quant. Spectrosc. Ra., 107, 105–119, 2007. 8666

Liljegren, J. C., Clothiaux, E. E., Mace, G. G., Kato, S., and Dong, X.: A new retrieval for cloud liquid water path using a ground-based microwave radiometer and measurements of cloud temperature, J. Geophys. Res., 106, 14485–14500, 2001. 8665

Mahesh, A., Walden, V. P., and Warren, S. G.: Ground-based infrared remote sensing of cloud properties over the Antarctic plateau. Part II: cloud optical depths and particle sizes, J. Appl. Meteorol., 40, 1279–1294, 2001. 8655

Marchand, R., Ackerman, T., Westwater, E. R., Clough, S. A., Pereira, K. C., and Liljegren, J. C.: An assessment of microwave absorption models and retrievals of cloud liquid water using clear-sky data, J. Geophys. Res., 108, 4773, doi:10.1029/2003JD003843, 2003. 8665, 8669

McFarquhar, G. M., Ghan, S., Verlinde, J., Korolev, A., Strapp, J. W., Schmid, B., Tomlinson, J. M., Wolde, M., Brooks, S. D., Cziczo, D., Dubey, M. K., Fan, J., Flynn, C., Gultepe, I., Hubbe, J., Gilles, M. K., Laskin, A., Lawson, P., Leaitch, W. R., Liu, P., Liu, X., Lubin, D., Mazzoleni, C., MacDonald, A.-M., Moffet, R. C., Morrison, H., Ovchinnikov, M., Shupe, M. D., Turner, D. D., Xie, S., Zelenyuk, A., Bae, K., Freer, M., and Glen, A.: Indirect and semi-direct aerosol campaign, Bull. Am. Meteorol. Soc., 92, 183–201, doi:10.1175/2010BAMS2935.1, 2011. 8655, 8659

Morrison, H., Zuidema, P., Ackerman, A. S., Avramov, A., de Boer, G.,Fan, J., Fridlind, A. M., Hashino, T., Harrington, J. Y., Luo, Y., Ovchinnikov, M., and Shipway, B.: Intercomparison of cloud model simulations of Arctic mixed-phase boundary layer clouds observed during SHEBA/FIRE-ACE, Journal of Advances in Modeling Earth Systems, 30, M06003, doi:10.1029/2011MS000066, 2011. 8654

Peppler, R. A., Long, C. N., Sisterson, D. L., Turner, D. D., Bahrmann, C. P., Christensen, S. W., Doty, K. J., Eagan R. C., Halter, T. D., Ivey, M. D., Keck, N. N., Kehoe, K. E., Liljegren, J. C., Macduf, M. C., Mather, J. H., McCord, R. A., Monroe, J. W., Moore, S. T., Nitschke, K. L., Orr, B. W., Perez, R. C., Perkins, B. D., Richardson, S. J., Sonntag, K. L., Voyles, J. W., and Wagener, R.: An overview of ARM program climate research facility data quality assurance, The Open Atmos. Sci. J., 2, 192–216, doi:10.2174/1874282300802010192, 2008. 8664

Pinto, J. O., Curry, J. A., and Intrieri, J. M.: Cloud-aerosol interactions during autumn over Beaufort Sea, J. Geophys. Res., 106, 15077–15098, doi:10.1029/2000JD900267, 2001. 8659

AMTD
5, 8653–8699, 2012

Rangno, A. L. and Hobbs, P. V.: Ice particles in stratiform clouds in the Arctic and possible mechanisms for the production of high ice concentrations, J. Geophys. Res., 106, 15065–15076, doi:10.1029/2000JD900286, 2001. 8655, 8663

Riedi, J., Marchant, B., Platnick, S., Baum, B. A., Thieuleux, F., Oudard, C., Parol, F., Nicolas, J.-M., and Dubuisson, P.: Cloud thermodynamic phase inferred from merged POLDER and MODIS data, Atmos. Chem. Phys., 10, 11851–11865, doi:10.5194/acp-10-11851-2010, 2010. 8658

Shupe, M. D.: Clouds at Arctic atmospheric observatories. Part II: thermodynamic phase characteristics, J Appl. Meteorol. Clim., 50, 645–661, doi:10.1175/2010JAMC2468.1, 2011. 8655

Shupe, M. D., Uttal, T., and Matrosov, S. Y.: Arctic cloud microphysics retrievals from surface-based remote sensors at SHEBA, J. Appl. Meteorol., 44, 1544–1562, 2005. 8655, 8672

Shupe, M. D., Matrosov, S. Y., and Uttal, T.: Arctic mixed-phase cloud properties derived from surface-based sensors at SHEBA, J. Atmos. Sci., 63, 697–711, 2006. 8655

Smith, W. S. and Kao, C. Y.: Numerical simulations of observed Arctic stratus clouds using a second-order turbulence closure model, J. Appl. Meteorol., 35, 47–59, 1996. 8654

Stamnes, K., Tsay, S. C., Wiscombe, W., and Jayaweera, K.: A numerically stable algorithm for discrete-ordinate-method radiative transfer in multiple scattering and emitting layered media, Appl. Optimizat., 27, 2502–2509, 1988. 8657

Strabala, K. I., Ackerman, S. A., and Menzel, W. P.: Cloud properties inferred from 8–12 µm data, J. Appl. Meteorol., 33, 212–229, 1994. 8658

Tietze, K., Riedi, J., Stohl, A., and Garrett, T. J.: Space-based evaluation of interactions between aerosols and low-level Arctic clouds during the spring and summer of 2008, Atmos. Chem. Phys., 11, 3359–3373, doi:10.5194/acp-11-3359-2011, 2011. 8655

Turner, D. D.: Arctic mixed-phase cloud properties from aeri lidar observations: algorithm and results from sheba, J. Appl. Meteorol., 44, 427–444, doi:10.1175/JAM2208.1, 2005. 8658, 8659, 8670

Turner, D. D. and Eloranta, E.: Validating mixed-phase cloud optical depth retrieved from infrared observations with high spectral resolution lidar, IEEE Geosci. Remote S., 5, 285–288, doi:10.1109/LGRS.2008.915940, 2008. 8655, 8670

Turner, D. D., Ackerman, S. A., Baum, B. A., Revercomb, H. E., and Yang, P.: Cloud phase determination using ground-based AERI observations at SHEBA, J. Appl. Meteorol., 42, 701–715, 2003. 8655, 8658

AMTD
5, 8653–8699, 2012

Uppala, S., Kållberg, P. W., Simmons, A. J., Andrae, U., Bechtold, V. D. C., Fiorino, M., Gibson, J. K., Haseler, J., Hernandez, A., Kelly, G. A., Li, X., Onogi, K., Saarinen, S., Sokka, N., Allan, R. P., Andersson, E., Arpe, K., Balmaseda, M. A., Beljaars, A. C. M., Berg, L. V. D., Bidlot, J., Bormann, N., Caires, S., Chevallier, F., Dethof, A., Dragosavac, M., Fisher, M., Fuentes, M., Hagemann, S., Hólm, E., Hoskins, B. J., Isaksen, L., Janssen, P. A. E. M., Jenne, R., McNally, A. P., Mahfouf, J.-F., Morcrette, J.-J., Rayner, N. A., Saunders, R. W., Simon, P., Sterl, A., Trenberth, K. E., Untch, A., Vasiljevic, D., Viterbo, P., and Woollen, J.: The ERA-40 re-analysis, Q. J. Roy. Meteor. Soc., 131, 2961–3012, 2005. 8666

van Diedenhoven, B., Fridlind, A. M., Ackerman, A. S., Eloranta, E. W., and McFarquhar, G. M.: An evaluation of ice formation in large-eddy simulations of supercooled Arctic stratocumulus using ground-based lidar and cloud radar, J. Geophys. Res.-Atmos., 114, D10203, doi:10.1029/2008JD011198, 2009. 8655

Verlinde, J., Harrington, J. Y., McFarquhar, G. M., Yannuzzi, V. T., Avramov, A.,d Greenberg, S., Johnson, N., Zhang, G., Poellot, M. R., Mather, J. H., Turner, D. D., Eloranta, E. W., Zak, B. D., Prenni, A. J., Daniel, J. S., Kok, G. L., Tobin, D. C., Holz, R., Sassen, K., Spangenberg, D., Minnis, P., Tooman, T. P., Ivey, M. D., Richardson, S. J., Bahrmann, C. P., Shupe, M., Demott, P. J., Heymsfield, A. J., and Schofield, R.: The mixed-phase Arctic cloud experiment, Bull. Am. Meteorol. Soc., 88, 205–221, 2007. 8655

Wang, X. and Key, J. R.: Recent trends in Arctic surface, cloud, and radiation properties from space, Science, 299, 1725–1728, 2003. 8654

Wang, X. and Key, J. R.: Arctic surface, cloud, and radiation properties based on the AVHRR polar pathfinder dataset. Part I: spatial and temporal characteristics, J. Climate, 18, 2558–2574, 2005. 8655

Warren, S. G. and Brandt, R. E.: Optical constants of ice from the ultraviolet to the microwave: a revised compilation, J. Geophys. Res., 113, D14220, doi:10.1029/2007JD009744, 2008. 8657, 8658

Wieliczka, D. M., Weng, S., and Querry, M. R.: Wedge shaped cell for highly absorbent liquids: infrared optical constants of water, Appl. Optimizat., 28, 1714–1719, 1989. 8657, 8664

Wiscombe, W. J.: Improved Mie scattering algorithms, Appl. Optimizat., 19, 1505–1509, 1980. 8657, 8660

Witte, H. J.: Airborne observations of cloud particles and infrared flux density in the Arctic, Master's thesis, University of Washington, Seattle, USA, 1968. 8655

AMTD
5, 8653–8699, 2012

Xiong, X., Lubin, D., Li, W., and Stamnes, K.: A critical examination of satellite cloud retrieval from AVHRR in the Arctic using SHEBA data, J. Appl. Meteorol., 41, 1195–1209, 2002. 8655
Zhao, C. and Garrett, T. J.: Ground-based remote-sensing of precipitation in the Arctic, J. Geophys. Res., 113, D14204, doi:10.1029/2007JD009222, 2008. 8660, 8661

AMTD
5, 8653–8699, 2012

Table 1. Site, instrument, resolution, and 95 % confidence accuracy of measurements used in this study.

Source	Instrument	Data	resolution	Accuracy
ROSE-GOME	Satellite Spectrometer	Stratospheric O_3 profile	6 h	5–10 %
GMD	Photometers	Surface ozone	1 h	2 %
NWS	Rawinsonde	Temperature Profile	12 h	3 K
NWS	Rawinsonde	Water vapor Profile	12 h	15 %
ARM	AERI	Surface Radiation	450 s	0.5 mW (m^2 sr cm^{-1})
ARM	Laser/Ceilometer	Cloud Base	36 s	7.6 m
ARM	MMCR Radar	Radar Reflectivity	36 s	0.5 dB
ARM	MMCR Radar	Cloud Top	36 s	45 m
ARM	MMCR Radar	Doppler velocity	36 s	0.1 m s^{-1}
ARM	MWR	Liquid water path	15 s	30 g m^{-2}

AMTD
5, 8653–8699, 2012

Table 2. Typical 95 % confidence retrieval errors for liquid and (ice) cloud r_e, τ, WP and N based on combined measurement and retrieval errors.

	Measurement	r_e	τ	WP	N
T_c	~ 3 K	8 %	15 %	12 %	21 %
T profile	5 %	1 %	7 %	6 %	7 %
H_2O vapor profile	15 %	1 %	1 %	1 %	3 %
I	$\sim 0.5\,\mathrm{mW\,(m^2\,sr\,cm^{-1})^{-1}}$	5 %	10 %	8 %	10 %
ΔH	~ 50 m (~ 20 %)				20 %
O_3	~ 100 ppb	1 %	1 %	1 %	3 %
σ	± 0.10				20 (45) %
Method		1 %	1 %	2 %	2 %
Total		10 %	20 %	16 %	38 (55) %

AMTD
5, 8653–8699, 2012

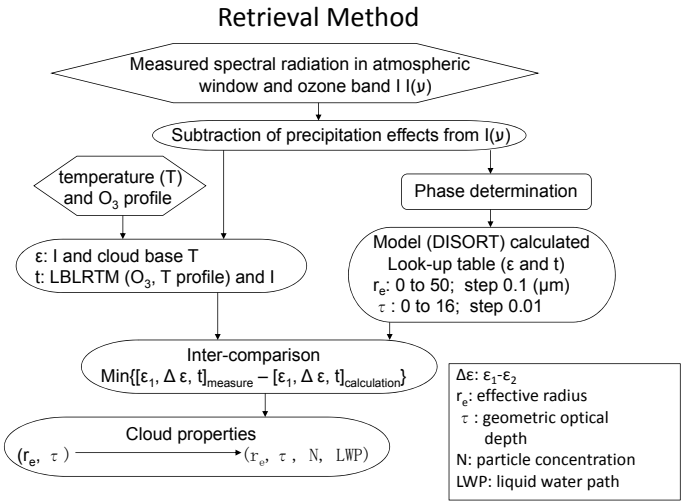

Fig. 1. Diagram illustrating the cloud property retrieval method. The parameters r_e, τ, ε, t, N and WP represent effective radius, visible optical depth, cloud emissivity, cloud transmittance, particle concentration and water path, respectively. Cloud phase is determined first based on cloud spectral emissivity and cloud base brightness temperature. A look-up table including ε and t for a range of r_e and τ is computed with DISORT for the corresponding phase. Calculated ε and t are obtained based on measurements. A minimization of the difference between calculated ε and t and values in the look-up table is used to obtain r_e and τ. Cloud N and WP are obtained based on a log-normal size distribution and the retrieved values of r_e and τ.

AMTD
5, 8653–8699, 2012

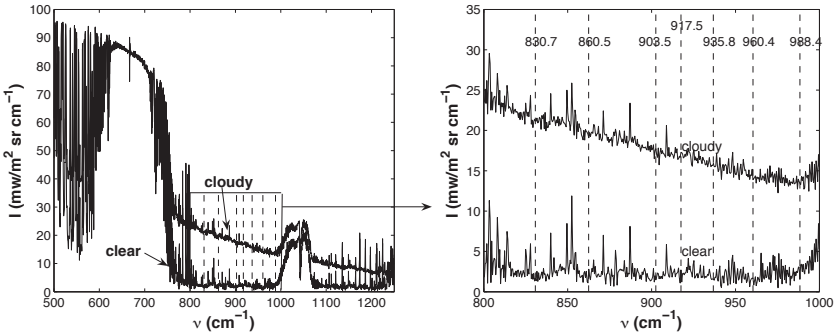

Fig. 2. Selected micro-windows in the atmospheric window, at which atmospheric gases absorption is particularly small. The upper and lower spectral radiation are for cloudy and clear conditions, respectively, measured at ARM NSA-AAO on 7 May 2001.

AMTD
5, 8653–8699, 2012

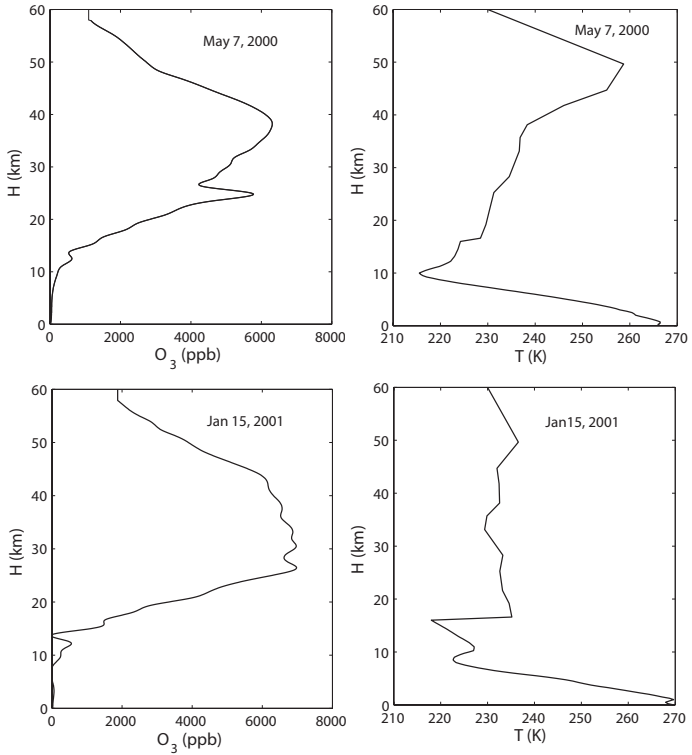

Fig. 3. Water and ice absorption efficiency Q_{abs} as a function of cloud particle effective size r_e at six different wavenumbers within atmospheric micro-windows where atmospheric gaseous absorption is particularly small.

AMTD
5, 8653–8699, 2012

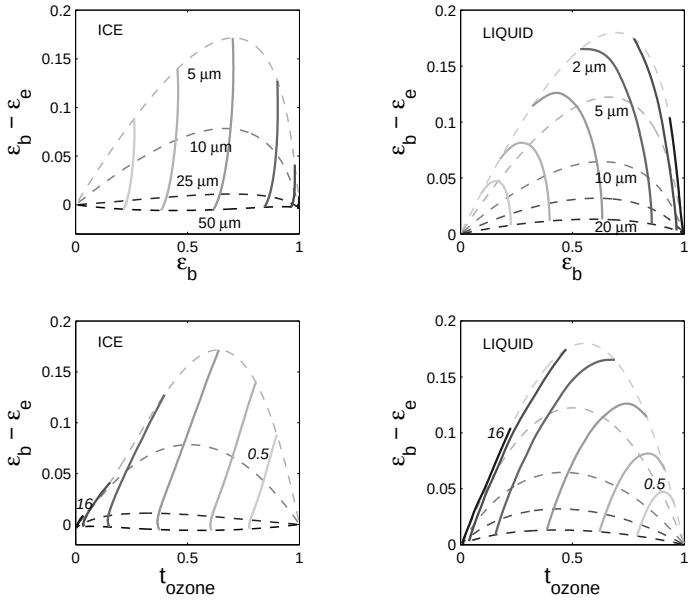

Fig. 4. "Arch plots" of split window cloud emssivity at 862.5 cm^{-1} (ε_b) and 935.8 cm^{-1} (ε_e), and cloud transmittance at 1040 cm^{-1} (t_{ozone}) for liquid and ice clouds, for a spread in effective radii r_e (dashed: as labeld) and optical depths τ (solid: 0.5, 1, 2, 4, 8, 16).

AMTD
5, 8653–8699, 2012

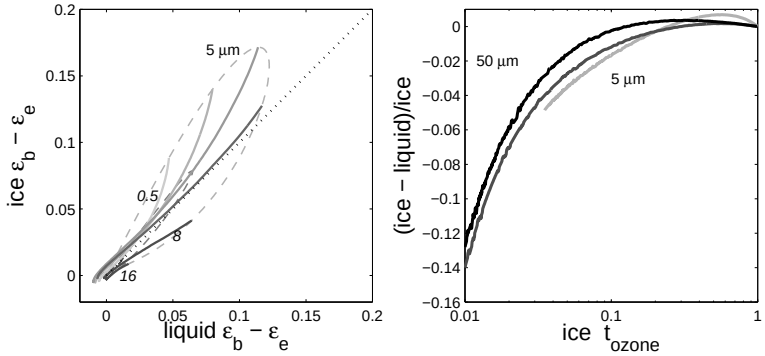

Fig. 5. Left: range of r_e (dashed: 5 and 10 μm) and τ (solid: 0.5, 1, 2, 4, 8, 16) associated with the split-window difference $\varepsilon_b - \varepsilon_e$, depending on whether a cloud is assumed to be liquid or ice. Right: the percent difference in transmissivity within the ozone band associated with cloud phase assumption.

AMTD
5, 8653–8699, 2012

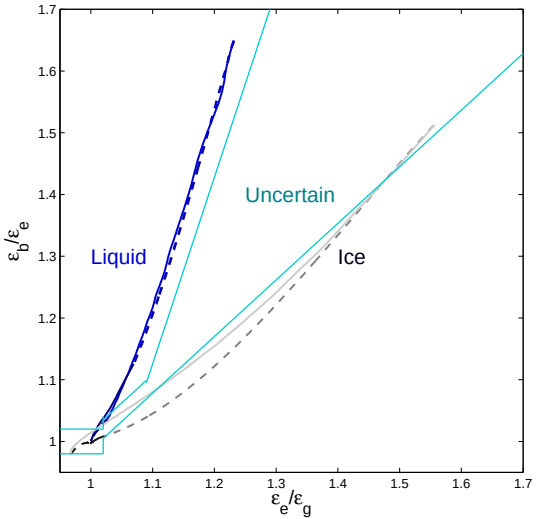

Fig. 6. An intercomparison of ratios of calculated cloud emissivities at 862.5 cm^{-1} (ε_b), 935.8 cm^{-1} (ε_e) and 988.4cm^{-1} (ε_g) for assumed liquid and ice clouds. Gray and blue lines lineate these ratios for a range of plausible parameter space in r_e and τ. Agua colored lines delineate the separation between diagnosed phase retrievals.

AMTD
5, 8653–8699, 2012

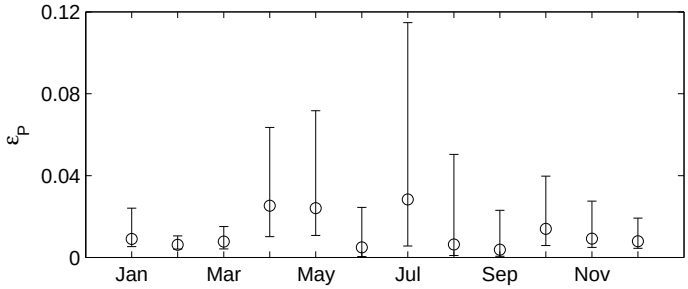

Fig. 7. Seasonal variation in retrieved precipitation emissivity at 934.5 cm^{-1} obtained at NSA-AAO between 2000 and 2003. Points are median values and bars the limits of the upper and lower quartiles.

AMTD
5, 8653–8699, 2012

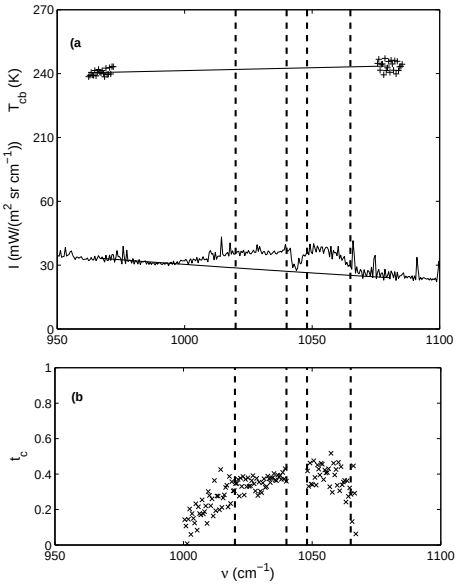

Fig. 8. Three steps are used to determine cloud transmittance in a 1038–1042 cm^{-1} microwindow. First (top), the brightness temperature T_{cb} at cloud base is calculated on both sides of the ozone band (970–990 cm^{-1} and 1070–1100 cm^{-1}), from which the cloud brightness temperature T_{cb} within the P and R branches of the ozone band is obtained using linear interpolation. Second (middle), the background radiance I_{bkg} from non-ozone sources is calculated from the estimated brightness temperatures. Third (bottom), the transmittance t in the P and R brances of the ozone band is calculated based on from the measured downwelling radiance I_{sky}, corrected for precipitation contributions, from $t = \left(I_{sky} - I_{bkg}\right)/I_{clear}$, where I_{clear} is the clear sky radiance. Transmittance values within the Q branch between 1040 cm^{-1} and 1048 cm^{-1} are estimated by interpolating from the two regions delimited by dashed lines. The data shown is from measurements at ARM NSA-AAO on 15 July 2000.

AMTD
5, 8653–8699, 2012

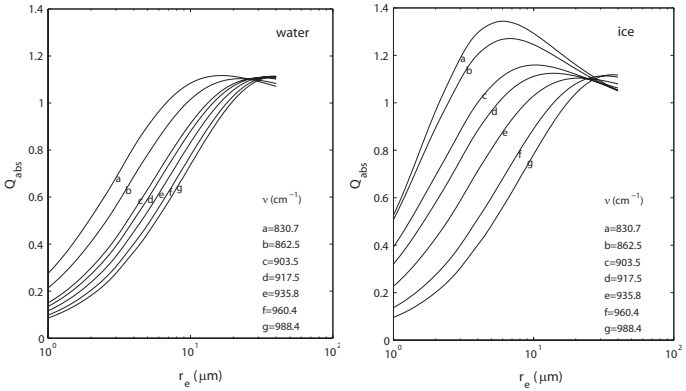

Fig. 9. Ozone (left) and temperature (right) profiles at Barrow, Alaska, obtained on 7 May 2000 (above) and 15 January 2001 (below).

AMTD
5, 8653–8699, 2012

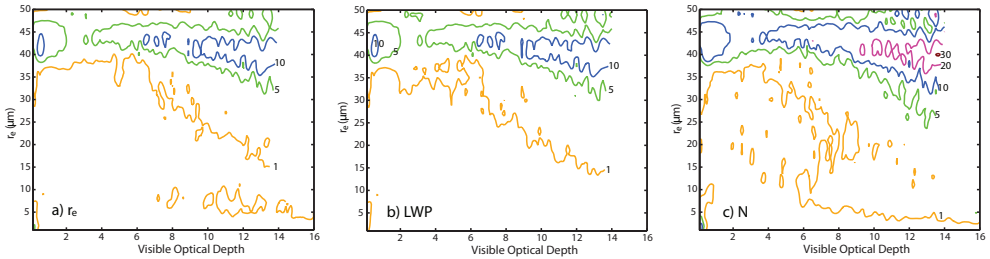

Fig. 10. Calculated uncertainties in retrievals of liquid cloud r_e, LWP and N that are associated only with the look-up table method.

AMTD
5, 8653–8699, 2012

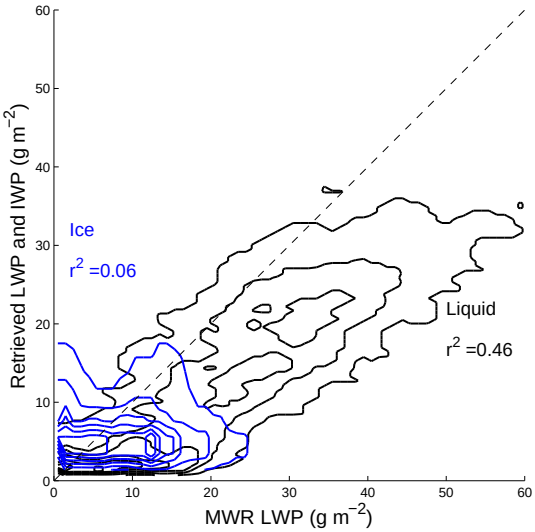

Fig. 11. Inter-comparison of retrieved and Microwave Radiometer (MWR) measured LWP.

AMTD
5, 8653–8699, 2012

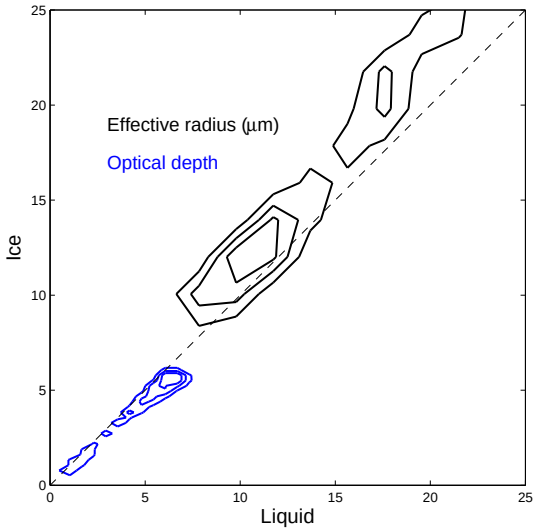

Fig. 12. Linear probability density distributions (contours) for retrieved clouds of "uncertain" phase depending on whether the optical properties are assumed to be those of ice or liquid.

AMTD
5, 8653–8699, 2012

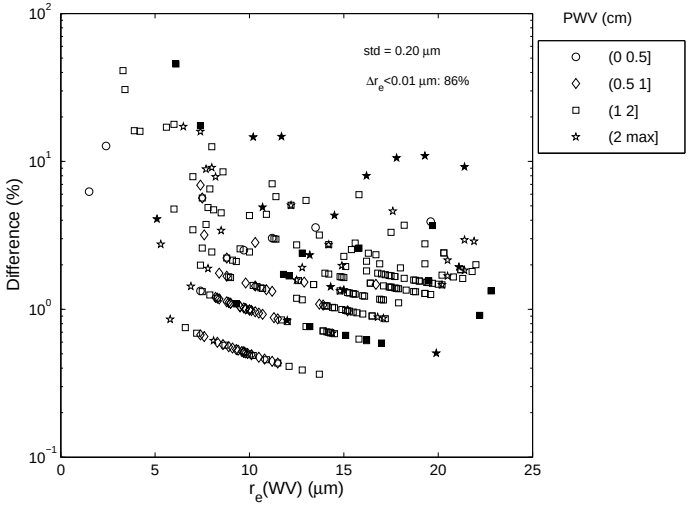

Fig. 13. Percent difference in retrievals of r_e associated with not subtracting water vapor contributions to measured downwelling radiance in emissivity calculations (Eq. 6), versus retrieved values with water vapor subtracted, as a function of the precipitable water vapor content (PWV) of the atmosphere. The only differences plotted are those in the 14 % of cases with differences in $r_e > 0.1$ μm. Negative differences are in closed circles.

AMTD
5, 8653–8699, 2012

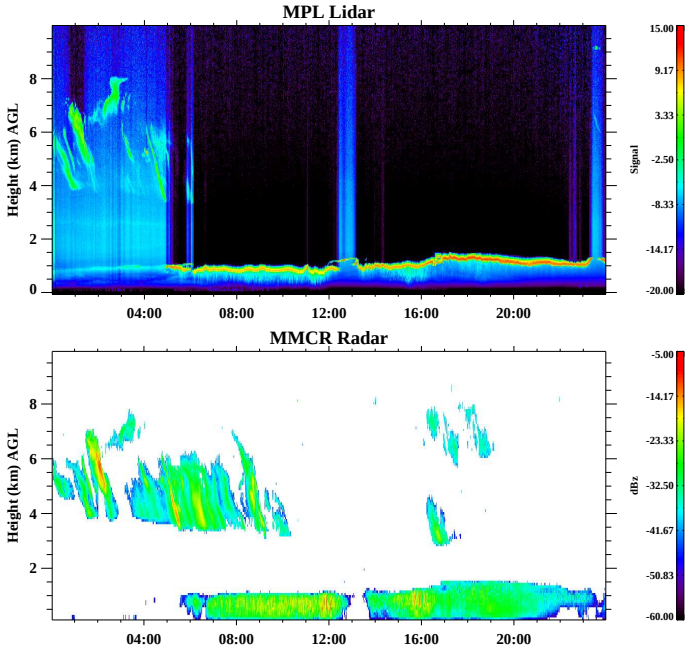

Fig. 14. Lidar and radar returns from NSA-AAO on 13 January 2001.

AMTD
5, 8653–8699, 2012

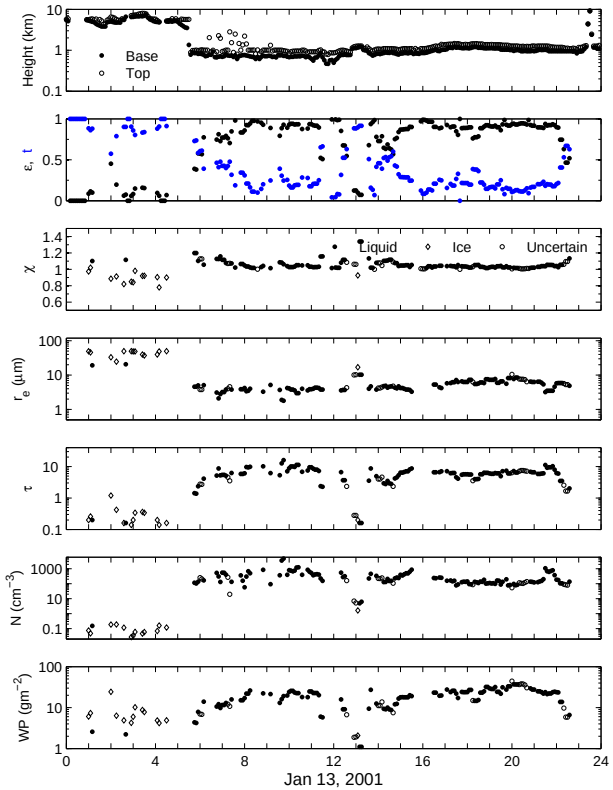

Fig. 15. Retrieved cloud boundaries H, emissivity (at 862.5 cm^{-1}) and transmissivity (at 1040 cm^{-1}), ratio of spectral slopes $\chi = (\varepsilon_b/\varepsilon_e)/(\varepsilon_e/\varepsilon_g)$, and cloud properties effective radius r_e, visible optical depth τ, particle number concentration N, and condensate water path WP, for the scene in Fig. 14 observed at NSA-AAO on 13 January 2001.

AMTD
5, 8653–8699, 2012

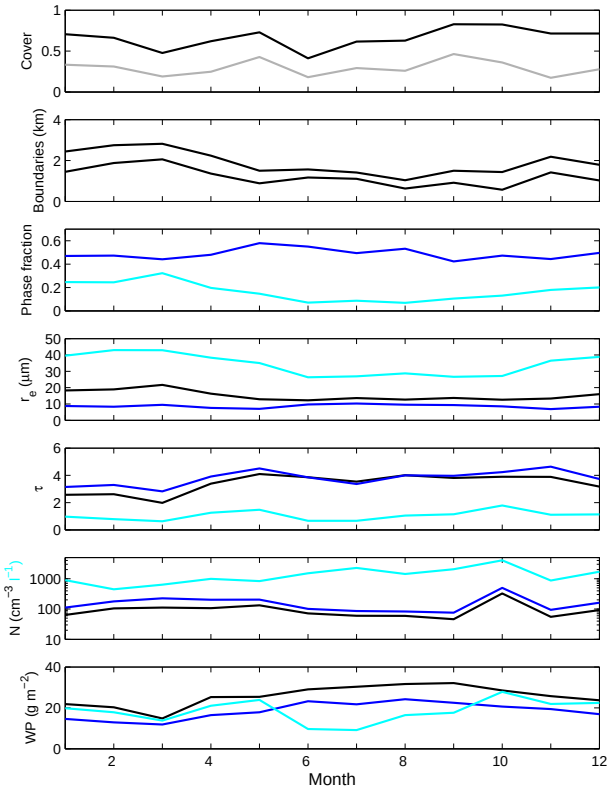

Fig. 16. Monthly averages of retrieved graybody cloud properties for the 2000 to 2003 time period at NSA-AAO. Top panel: retrieved cloud cover of all (black) and graybody (gray) clouds. Lower panels: for graybody clouds, cloud boundaries, fraction of clouds identified as liquid (blue) or ice (cyan), cloud particle effective radius r_e of liquid, ice and all (black) clouds, cloud optical depth τ, cloud particle number concentration (liquid (cm^{-3}), ice (l^{-1}), and water path WP.

AMTD
5, 8653–8699, 2012